

# Bayesian adjustment for preferential testing in estimating infection fatality rates, as motivated by the COVID-19 pandemic

Harlan Campbell<sup>1</sup>, Perry de Valpine<sup>2</sup>, Lauren Maxwell<sup>3</sup>,  
Valentijn M.T. de Jong<sup>4</sup>, Thomas P.A. Debray<sup>4,5</sup>,  
Thomas Jaenisch<sup>3,6</sup>, Paul Gustafson<sup>1</sup> \*

September 4, 2022

---

\*1. Department of Statistics, University of British Columbia, BC, Canada; 2. Department of Environmental Science, Policy, and Management, University of California, Berkeley, CA, USA; 3. Heidelberg Institute for Global Health, Heidelberg University Hospital, Heidelberg, Germany; 4. Julius Center for Health Sciences and Primary Care, University Medical Center Utrecht, Utrecht University, Utrecht, the Netherlands; 5. Cochrane Netherlands, Julius Center for Health Sciences and Primary Care, University Medical Center Utrecht, Utrecht University, Utrecht the Netherlands; 6. Department of Epidemiology, Colorado School of Public Health, CO, USA; This work was supported by the European Union's Horizon 2020 research and innovation programme under ReCoDID grant agreement N° 825746 and by the Canadian Institutes of Health Research, Institute of Genetics (CIHR-IG) under Grant Agreement N° 01886-000. We also wish to thank Joe Watson for his input early on and expertise on preferential sampling,

## Abstract

A key challenge in estimating the infection fatality rate (IFR) is determining the total number of cases. The total number of cases is not known because not everyone is tested but also, more importantly, because tested individuals are not representative of the population at large. We refer to the phenomenon whereby infected individuals are more likely to be tested than non-infected individuals, as “preferential testing.” An open question is whether or not it is possible to reliably estimate the IFR without any specific knowledge about the degree to which the data are biased by preferential testing. In this paper we take a partial identifiability approach, formulating clearly where deliberate prior assumptions can be made and presenting a Bayesian model, which pools information from different samples. When the model is fit to European data obtained from seroprevalence studies and national official COVID-19 statistics, we estimate the overall COVID-19 IFR for Europe to be 0.47%, 95% C.I. = [0.34%, 0.63%].

*Keywords:* selection bias, partial identification, evidence synthesis.

# 1 Introduction

If someone is infected with severe acute respiratory syndrome coronavirus 2 (SARS-CoV-2), the pathogen that causes COVID-19, how likely is that person to die of COVID-19? This simple question is surprisingly difficult to answer.

The “case fatality rate” (CFR) is a common measure that quantifies the mortality risk in a certain population, and is given by the ratio of deaths ( $D$ ) over confirmed cases ( $CC$ ) during a specific time period. However, because many COVID-19 cases are never diagnosed, the CFR almost certainly overestimates the true lethality of the virus. Instead, the better answer is captured by the infection fatality rate (IFR) (Kobayashi et al., 2020; Wong et al., 2013). The IFR, also a simple ratio, differentiates itself from the CFR by considering all cases, including the asymptomatic, undetected and misdiagnosed infections, in the denominator. For instance, if 20 individuals die of the disease in a population with 1,000 infections, then the IFR is  $20 / 1000 = 0.02 = 2\%$ .

Evidently, a key challenge in calculating the IFR is determining the true total number of cases. The total number of cases ( $C$ ) is not known because not everyone is tested in the population ( $P$ ). A naïve estimate of the IFR might take this into account by simply considering the number of tests ( $T$ ) and estimating the number of cases as:  $C \approx (CC/T) \times P$ . However, diagnostic tests are often selectively initiated, such that tested individuals are not representative of the population at large.

In most countries/jurisdictions, those with classic COVID-19 symptoms (e.g. fever, dry cough, loss of smell or taste) are much more likely to be tested than those without symptoms. Due to this severity bias, the reported number of cases likely includes mostly people whose symptoms were severe enough to be tested and excludes the vast majority of those who are mildly- or asymptomatic. Even when testing is made equally available to all

individuals (e.g., Bendavid et al. (2020)), there is potential for “selection bias” if people who have reason to believe they are infected are more likely to volunteer to be tested. We refer to the phenomenon whereby infected individuals are more likely to be tested than non-infected individuals, as “preferential testing.” (Hauser et al. (2020) and others use the term “preferential ascertainment.”)

If the degree of preferential testing in a particular sample is of known magnitude, bias adjustment can be achieved by appropriately altering the estimated rate of infection and its uncertainty interval. However, the degree of preferential testing is typically unknown and likely highly variable across different jurisdictions. An open question is whether or not it is possible to reliably estimate the IFR without any specific information about the degree to which the data are biased by preferential testing. And, if we have some samples for which testing is representative and others which are subject to some unknown bias from preferential testing, is it better to use only the representative data or to combine both kinds of data in a joint analysis? In this paper, we address these important questions by considering a Bayesian hierarchical model for estimation of the IFR. We demonstrate with an application in which we fit the model to European data from seroprevalence studies and national official COVID-19 statistics.

Bayesian models have been previously used in similar situations. For example, Presanis et al. (2009) conduct Bayesian inference to estimate the severity of pandemic H1N1 influenza. More recently, Rinaldi and Paradisi (2020), and Hauser et al. (2020) use Bayesian models for disease dynamics in order to estimate the severity of COVID-19. To address the issue of preferential testing bias, Hauser et al. (2020) apply susceptible-exposed-infected-removed (SEIR) compartmental models to age-stratified data and, in order to establish parameter identifiability, assume that all cases of infected patients aged 80 years and older

are confirmed cases. The Bayesian model we propose is more general and allows one to obtain appropriate point and interval estimates for the IFR with varying degrees of prior knowledge about the magnitude of preferential testing and the distribution of other explanatory factors (e.g. age, healthcare capacity).

This paper is structured as follows. In Section 2, we introduce required notation, discuss distributional assumptions and review key issues of identifiability. In Section 3, we formulate our Bayesian model and present a small illustrative example. In Section 4, we describe how the model can be scaled for larger populations and can incorporate covariates. In Section 5, we present a simulation study and in Section 6, we present an analysis of COVID-19 data from Europe. We conclude in Section 7.

## 2 Notation, distributions, and issues of (un)identifiability

### 2.1 Notation and distributions

Suppose we have data from  $K$  independent groups (i.e., countries or jurisdictions) from a certain fixed period of time. For group  $k$  in  $1, \dots, K$ , let:

- $P_k$  be the population size (i.e., the total number of individuals at risk of infection);
- $T_k$  be the total number of people tested;
- $CC_k$  be the total number of confirmed cases resulting from the tests; and
- $D_k$  be the total number of observed deaths attributed to infection.

We do not observe the following latent variables. For the  $k$ -th group, let:

- $C_k$  be the total number of infected people (cases) in the population;
- $IR_k$  be the true infection rate (proportion of the population which is infected), which is the expected value of  $C_k/P_k$ ;
- $IFR_k$  be the true underlying infection fatality rate (IFR), which is the expected value of  $D_k/C_k$ .

Therefore, we assume that:

$$C_k \sim \text{Binom}(P_k, IR_k), \quad \text{and:} \quad (1)$$

$$D_k|C_k \sim \text{Binom}(C_k, IFR_k), \quad (2)$$

where, in the  $k$ -th group, the unknown number of infections,  $C_k$ , and the known number of deaths,  $D_k$ , each follow a binomial distribution. Note that there are latent variables on both the left hand side and the right hand side of (1).

For each group,  $CC_k$  is recorded, instead of  $C_k$ . Even in the absence of preferential testing,  $CC_k$  will be smaller than  $C_k$  because not everyone is tested. In other words, the confirmed cases ( $CC$ ) are a subset of the total cases ( $C$ ). We assume that the distribution of the confirmed cases depends only on the actual infection rate ( $C/P$ ) and the testing rate ( $T/P$ ) but not on the infection fatality rate ( $D/C$ ) or other information. In other words, we assume that the conditional distribution of  $(CC|C, T, P, D)$  is identical to the conditional distribution of  $(CC|C, T, P)$ .

This assumption is similar to the assumption of “non-differential” exposure misclassification in measurement error models and may or may not be realistic; see De Smedt et al. (2018). For example, COVID-19 is thought to be deadlier amongst the elderly. If this is

true, the non-differential preferentiality assumption would fail if elderly individuals were just as likely to be infected as others, yet more likely to be tested (given covariates).

The goal is to draw inference on the relationship between the number of deaths,  $D$ , and the number of cases,  $C$ , having only data on  $D$ ,  $CC$ ,  $P$ , and  $T$ . This is particularly challenging since the number of confirmed cases in each group may be subject to an unknown degree of preferential testing.

In the absence of any preferential testing, if one assumes that the population sizes are finite, then the number of confirmed cases will follow a hyper-geometric distribution (Prochaska and Theodore, 2018). The hyper-geometric distribution describes the probability of  $CC_k$  confirmed cases amongst  $T_k$  tests (without any individuals being tested more than once), from a finite population of size  $P_k$  that contains exactly  $C_k$  cases. Wallenius' *non-central* hyper-geometric is a generalization of the hyper-geometric distribution whereby testing is potentially biased with either cases or non-cases more likely to be tested (Fog, 2008). We therefore consider the distribution of  $CC_k|C_k$  as following a non-central hyper-geometric distribution:

$$CC_k|C_k \sim NCHyperGeo(C_k, P_k - C_k, T_k, \phi_k), \quad (3)$$

where the degree of preferential testing corresponds to the  $\phi_k$  non-centrality parameter. When  $\phi_k > 1$ , cases (i.e., infected individuals) are more likely to be tested than non-cases (i.e., non-infected individuals); when  $\phi_k < 1$ , cases are less likely to be tested than non-cases. When  $\phi_k = 1$ , we have that the probability of being tested is equal for both cases and non-cases, and the non-central hyper-geometric distribution reduces to the standard hyper-geometric distribution. In this parameterization, the  $\phi_k$  parameter can be interpreted as an odds ratio: the odds of a case being tested vs. the odds of a non-case being tested.

## 2.2 Partial identifiability

Given the assumptions detailed above, for each of the  $K$  groups, there are three unknown parameters (latent states),  $IR_k$ ,  $IFR_k$  and  $\phi_k$ , that must be estimated for every two observed quantities ( $D_k/P_k$  and  $CC_k/T_k$ ). This suggests that a unique solution may not be attainable without additional external data or prior information.

The problem at hand is sufficiently rich and complex that forming intuition about the information-content of the data is challenging. In the Appendix (Section 8.1), we consider, in depth, an asymptotic argument for *partial identifiability*. We determine that, depending on the range and heterogeneity in the degree of preferential testing across groups, the data can contribute substantial information about the infection fatality rate. Data from any single group may only be weakly informative about the IFR, in the sense that only lower and upper bounds for the IFR are estimable. However, we show that in some circumstances there is very considerable sharpening of information when these bounds are combined across groups, provided it is *a priori* plausible that the IFR heterogeneity across groups is modest.

## 3 A Bayesian model for small- $P$ data and an illustrative example

### 3.1 A Bayesian model for small- $P$ data

Bayesian models work well for dealing with partially identifiable models; see Gustafson (2010). We describe a Bayesian model which assumes standard Gaussian random-effects allowing both the infection rate (IR) and infection fatality rate (IFR) to vary between



groups with:

$$g(IFR_k) \sim \mathcal{N}(\theta, \tau^2), \quad \text{and} \quad (4)$$

$$g(IR_k) \sim \mathcal{N}(\beta, \sigma^2), \quad (5)$$

for  $k$  in  $1, \dots, K$ , where  $\theta$  is the parameter of primary interest,  $\tau^2$  represents between group IFR heterogeneity,  $\beta$  represents the mean  $g(\text{infection rate})$ ,  $\sigma^2$  describes the variability in infection rates across the  $K$  groups, and  $g()$  is a given link function. For mathematical convenience, we will adopt the complimentary log-log link function though there are many sensible choices. Note that, alternatively, a simpler “fixed-effects” version of the model arises by setting  $\tau = 0$  such that  $g(IFR_k) = \theta$ , for  $k = 1, \dots, K$ .

Putting together the assumptions for  $p(D_k|IFR_k, C_k)$ ,  $p(CC_k|T_k, P_k, C_k, \phi_k)$  and  $p(C_k|P_k, IR_k)$  defined in Section 2.1 along with prior distributions, Bayes’ Law takes the form:

$$\begin{aligned} p((\theta, \tau^2, \beta, \sigma^2, C, IFR, IR, \phi)|\text{data}) &\propto p(\text{data}|\theta, \tau^2, \beta, \sigma^2, C, IFR, IR, \phi) \\ &\times p(\theta, \tau^2, \beta, \sigma^2, C, IFR, IR, \phi) \\ &= \left( \prod_{k=1}^K p(D_k|IFR_k, C_k)p(CC_k|T_k, P_k, C_k, \phi_k)p(C_k|P_k, IR_k)p(IFR_k|\theta, \tau^2)p(IR_k|\beta, \sigma^2) \right) \\ &\times p(\theta)p(\tau^2)p(\beta)p(\sigma^2)p(\phi). \end{aligned} \quad (6)$$

We are left to define prior distributions for the unknown parameters:  $\theta$ ,  $\tau^2$ ,  $\beta$ ,  $\sigma^2$ , and  $\phi$ .

Our strategy for priors on IR and IFR is to assume uninformative priors for the mean of IFR and of IR and for the variance of IR but a strongly informative prior for the variance of IFR. This strategy reflects the assumption that the infection fatality rate varies across jurisdictions much less than the infection rate itself (especially after accounting

for population level sources of heterogeneity; see Section 4.2). The priors are set accordingly:  $g^{-1}(\theta) \sim \text{Uniform}(0, 1)$ ;  $g^{-1}(\beta) \sim \text{Uniform}(0, 1)$ ;  $\tau \sim \text{half-}\mathcal{N}(0, 0.01)$ ; and  $\sigma \sim \text{half-}\mathcal{N}(0, 1)$ .

The only remaining component is  $p(\phi)$ . Our strategy for a prior on the degree of preferential testing is to assume that cases are more likely to be tested than non-cases (i.e.,  $\phi_k > 1$ ), that all values of  $\phi_k$  are equally likely across jurisdictions, and that there is an upper bound,  $1 + \gamma$ , on degree of preferentiality. For the upper bound parameter,  $\gamma$ , we assume an exponential prior, such that:

$$\phi_k \sim \text{Uniform}(1, 1 + \gamma), \quad \text{for } k \text{ in } 1, \dots, K; \text{ and } \gamma \sim \text{Exp}(\lambda = 0.5).$$

The prior specification therefore assumes that the uniform range of possible values for  $\phi_k$  is itself unknown. Setting  $\lambda = 0.5$  implies that, *a priori*, a reasonable value for the  $\phi_k$  odds ratio is 2, (i.e., since  $E(\gamma) = 1/\lambda$  and  $E(\phi_k) = (1 + (\gamma + 1))/2$ ). In the Appendix (Section 8.3), we illustrate this approach with an application to the artificial dataset introduced earlier in Table 4.

In some scenarios, we might have some groups for which  $\phi_k$  is known and equal to 1 (i.e., have data from some samples where testing is known to be truly random). Without loss of generality, suppose this subset is the first  $k'$  studies, such that for  $k = 1, \dots, k'$ , we have  $\phi_k = 1$ . We will use this approach in the Europe data analysis (Section 6), in which we assume  $\phi_k$  is known and equal to 1 for data from representative seroprevalence studies.

We must emphasize that the performance of any Bayesian estimator will depend on the choice of priors and that this choice can substantially influence the posterior when few data are available (Berger, 2013; Lambert et al., 2005). The priors described here represent a scenario where there is little to no *a priori* knowledge about the  $\theta$ ,  $\beta$ , and  $\phi$  model parameters. Inference would no doubt be improved should more informative priors

be specified based on probable values for each of these parameters. We briefly consider the impact of priors in the simulation study in Section 5, where we look to different values for  $\lambda$ .

We must also emphasize that, due to the partial identifiability issues (Section 2.2), a delicate trade-off exists between the priors for the  $\tau$  and  $\phi$  parameters. For instance, if large values of  $\tau$  are made *a priori* plausible, then the posterior estimates of the  $\phi$  parameters will be driven downwards towards 1 (due to the  $\gamma \sim \text{Exp}(\lambda = 0.5)$  prior). A relatively homogeneous across-group IFR is central to identifiability and, as such, the aforementioned “fixed-effects” version of the model (essentially equivalent to fixing  $\tau = 0$ ) may be more feasible in situations when identification is particularly challenging (e.g., when there is very little prior knowledge about the  $\theta$ ,  $\beta$ , and  $\phi$  model parameters).

## 4 A Bayesian model for large- $P$ data

### 4.1 Distributional approximations

When populations are large, we can simplify our model (in order to reduce the computational complexity), by replacing the non-central hyper-geometric distribution with a binomial distribution as follows:

$$CC_k \sim \text{Binom}(T_k, 1 - (1 - IR_k)^{\phi_k}), \quad (7)$$

$$C_k \sim \text{Binom}(P_k, IR_k), \quad (8)$$

$$D_k | C_k \sim \text{Binom}(C_k, IFR_k), \quad (9)$$

for  $k$  in  $1, \dots, K$ . Note that the  $\phi_k$  parameter above no longer corresponds to an odds ratio, yet the interpretation is similar. The odds ratio (OR) describing the association between testing status and infection status is

$$\log(OR) = \log(1 - (1 - IR)^\phi) - \phi \times \log(1 - IR) - \log(IR) + \log(1 - IR).$$

For fixed  $IR$ , approximating this with a Taylor series in  $\log(\phi)$ , about zero, gives:  $\log(OR) \approx c_{IR} \log(\phi)$ , where  $c_{IR} = -\log(1 - IR)/IR$ . Note that  $c_{IR} \rightarrow 1$  as  $IR \rightarrow 0$ . Therefore, in the rare-infection realm,  $\phi$  is indeed approximately the odds ratio for testing and infection status.<sup>1</sup>

We can further simplify by marginalizing over the cases. Since we have the distribution of  $C_k$  and the conditional distribution of  $D_k$  given  $C_k$ , and since both of these are binomials, we have that unconditionally:

$$D_k \sim \text{Binom}(P_k, IFR_k \times IR_k). \quad (10)$$

## 4.2 Including group-level covariates

The proposed model can be expanded to include covariates specified as covariates at the group level. These might be factors that are correlated with the probability of becoming infected with SARS-Cov-2, with the probability of being tested, with the accuracy of the test, and/or with the probability of dying from infection.

Suppose that  $X_{[1]k}, \dots, X_{[h]k}$  are  $h$  different group-level covariates that explain the  $k$ -th

---

<sup>1</sup>We could have alternatively substituted the non-central hyper-geometric distribution with the known Gaussian asymptotic approximation to the non-central hyper-geometric (Stevens, 1951). However, the Gaussian approximation requires solving quadratic equations and therefore, might not necessarily help reduce the computational complexity of our model; see Sahai and Khurshid (1995).

group’s infection rate, and that  $Z_{[1]k}, \dots, Z_{[q]k}$  are  $q$  different covariates that explain the  $k$ -th group’s IFR. Then these can be incorporated as follows:

$$g(IR_k) \sim \mathcal{N}(\beta + \beta_1 X_{[1]k} + \dots + \beta_h X_{[h]k}, \sigma^2), \quad (11)$$

$$g(IFR_k) \sim \mathcal{N}(\theta + \theta_1 Z_{[1]k} + \dots + \theta_q Z_{[q]k}, \tau^2). \quad (12)$$

Age is a key factor for explaining the probability of COVID-19-related death. One might therefore consider median age of each group as a predictor for the IFR, or perform analyses that are stratified by different age groups (Onder et al., 2020). The latter strategy has, for instance, been recommended to make accurate predictions for respiratory infections (Pellis et al., 2020). With regards to the infection rate, time since first reported infection, or time between first reported infection and the imposition of social distancing measures might be predictive (Anderson et al., 2020).

### 4.3 MCMC

For the large-P model, Markov chain Monte carlo (MCMC) mixing can be slow because different combinations of  $\phi_k$ ,  $\text{cloglog}(IR_k)$  and  $\text{cloglog}(IFR_k)$  can yield similar model probabilities. This is related to the identifiability issues discussed in the Appendix (Section 8.1). To improve mixing and reduce computational time for the simulation study, we wrote this model in the nimble package (de Valpine et al., 2017), which supports an extension of the modeling language used in JAGS and makes it easy to configure samplers and provide new samplers. Details of the MCMC implementation for nimble are presented in the Appendix (Section 8.3). We also implemented the large-P model in the popular Stan package which employs Hamiltonian MCMC algorithms (Carpenter et al., 2017).

## 5 Simulation study

### 5.1 Design

We conducted a simulation study in order to better understand the operating characteristics of the proposed model. Specifically, we wished to evaluate the frequentist coverage of the credible interval for  $\theta$ , and investigate the impact of the chosen prior for the magnitude of preferential testing (i.e., the impact of selecting different values for  $\lambda$ ). As emphasized in Gustafson et al. (2009), the average frequentist coverage of a Bayesian credible interval, taken with respect to the prior distribution over the parameter space, will equal the nominal coverage. This mathematical property is unaffected by the lack of identification. However, the variability of coverage across the parameter space is difficult to anticipate and could be highly affected by the choice of prior. For example, we might expect that, in the absence of preferential testing (i.e., when  $\gamma = 0$ ), coverage will be lower than the nominal rate. However, if this is the case, coverage will need to be higher than the nominal rate when  $\gamma > 0$ , so that the “average” coverage (taken with respect to the prior distribution over the parameter space) is nominal overall.

We simulated datasets with  $K = 20$  and  $k' = 8$ . For  $k = 1, \dots, 8$ , population sizes were obtained from a  $NegBin(20000, 1)$  distribution with a mean of 20,000 and for  $k = 9, \dots, 20$ , population sizes were obtained from a  $NegBin(200000, 1)$  distribution. Parameter values were as follows:  $\theta = cloglog(0.02) = -3.90$ ,  $\beta = cloglog(0.20) = -1.50$ ,  $\tau^2 = 0.005$  and  $\sigma^2 = 0.25$ . The testing rate for each population was obtained from a  $Uniform(0.01, 0.10)$  distribution so that the proportion of tested individuals in each population ranged from 1% to 10%. We considered eight values of interest for  $\gamma$ : 0, 1, 4, 11, 22, 34, 52, and 80 (for simulation); and three different values of interest for  $\lambda$ : 0.25, 0.50, and 0.75 (for estimation).

The number of confirmed cases ( $CC_k$ ) were simulated from Wallenius’ non-central hypergeometric distribution as detailed in Section 2.1. Note that with high  $\gamma$  levels, the vast majority of tests will be positive (when  $\gamma = 52$ , positivity is about 75%; when  $\gamma = 80$ , positivity is about 80%). The 12 “unknown”  $\phi_k$  values, for  $k$  in  $9, \dots, 20$ , simulated from a  $Uniform(1, \gamma + 1)$  distribution.

We fit three models to each unique dataset:  $M_1$ ,  $M_2$ , and  $M_3$ . All three models follow the same large- $P$  framework detailed in Section 4.1 but consider different subsets of the data. The  $M_1$  model uses only data from the samples for which  $\phi_k$  is unknown, i.e.,  $\{P_k, T_k, CC_k, \text{ and } D_k\}$  for  $k$  in  $9, \dots, 20$ . The  $M_2$  model considers the data from all the groups, i.e.,  $\{P_k, T_k, CC_k, \text{ and } D_k\}$  for  $k$  in  $1, \dots, 20$ . Finally, the  $M_3$  model uses only data from the samples for which  $\phi_k$  is known and equal to 1, i.e.,  $\{P_k, T_k, CC_k, \text{ and } D_k\}$  for  $k$  in  $1, \dots, 8$ . To be clear, the  $M_2$  and  $M_3$  models make the assumption of (correctly) known  $\phi_k = 1$  for  $k = 1, \dots, 8$ .

We simulated 200 unique datasets and, for each, fit the three different models. The  $M_1$  and  $M_2$  models are fit 24 different times ( $= 3 \times 8$ ) for each unique dataset, each time with  $\lambda$  assuming one of the three values of interest, and with one of the eight different sets of  $CC_k$  numbers (for  $k$  in  $9, \dots, 20$ ), corresponding to the eight  $\gamma$  values. For each case, we recorded the width of the 90% highest posterior density (HPD) CI for  $\theta$  and whether or not the CI contained the target value of  $cloglog(0.02) = -3.90$ .

We specifically chose to conduct 200 simulation runs so as to keep computing time within a reasonable limit while also reducing the amount of Monte Carlo standard error (MCSE) to a reasonably small amount (for looking at coverage with  $1 - \alpha = 0.90$ , MCSE will be approximately  $\sqrt{0.90(1 - 0.90)/200} \approx 0.02$ ); see Morris et al. (2019). For each simulation scenario, we used nimble to obtain 100,000 MCMC draws from the posterior

(20% burn-in, thinning of 50).

## 5.2 Results

Figure 1 plots the simulation study results. First, note that coverage for model  $M_3$  (based on only the unbiased data) is approximately 0.90 as expected; see dotted black line on Figure 1 lower-left panel. Results from the  $M_1$  model (upper panels, dashed lines) show that the model provides at or above nominal coverage when  $\gamma = 1$ , but not otherwise. In contrast, results from the  $M_2$  model (lower panels, solid lines) show that the model provides at or above nominal coverage for a wide range of  $\gamma$  values. This suggests that, when some representative data is available, appropriate estimation is achievable even in the presence of a substantial and unknown amount of preferential testing. When  $\gamma = 11$ , the odds (on average) for a case to be tested are more than six times the odds for a non-case (the average  $\phi_k$  value is equal to  $(1 + (\gamma + 1))/2$ ), and yet the model is able to appropriately adjust. Note that when  $\gamma = 0$ , coverage is well below nominal levels. This is likely due to the fact that the true parameter sits on the boundary of the parameter space.

Results from the  $M_2$  and  $M_3$  models suggest that for a given range of  $\gamma$  values, the  $M_2$  model (which makes use of all the data) is preferable to the  $M_3$  model (which uses data only from those samples where testing is known to be representative/random). Both achieve nominal coverage, but  $M_2$  does so with narrower interval widths. However, there is a limit to the “added value” that the “non-representative” data provide. For example, for  $\gamma \geq 22$ ,  $M_3$  intervals are narrower compared to  $M_2$  intervals (for all  $\lambda$ ).

Finally, note that overall the interval width is much narrower for  $M_2$  relative to  $M_1$  (compare dashed lines in lower-right panel to those in upper-right panel of Figure 1) which confirms that the  $k' = 8$  representative samples are very valuable for reducing the uncer-



tainty around  $\theta$ . With regards to the COVID-19 pandemic, this emphasizes the importance of conducting some amount of “unbiased testing” even if the sample sizes are relatively small; see Cochran (2020).

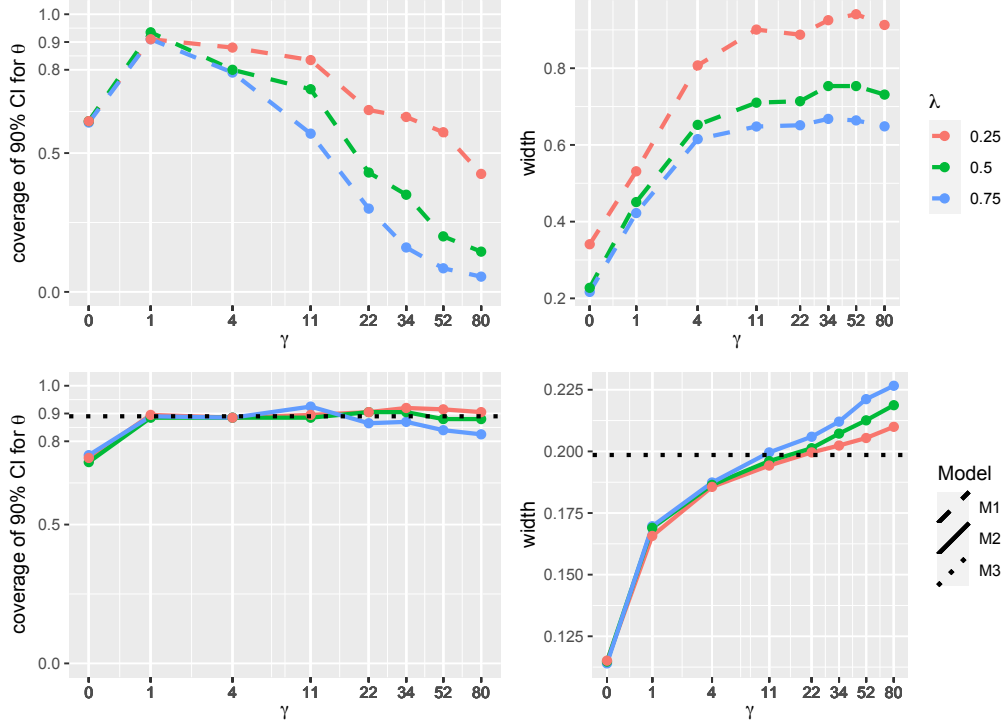


Figure 1: Simulation study results. Left-hand panels correspond to frequentist coverage and right-hand panels plot average interval width. The dotted lines corresponds to the  $M_1$  model, the solid lines correspond to the  $M_2$  model and the dashed line corresponds to the  $M_3$  model.

## 6 Application- IFR of COVID-19 in Europe

Reducing uncertainty around the severity of COVID-19 is of great importance to policy makers and the public (Ioannidis, 2020b; Lipsitch, 2020). Comparisons between the COVID-19 and seasonal influenza IFRs have impacted the timing and degree of social distancing measures and highlighted the need for more accurate estimates for the severity of both viruses (Faust, 2020). The current lack of clarity means that policy makers are unsure if cross-population differences are related to clinically relevant heterogeneity (i.e., due to large  $\tau^2$ ) or to spurious heterogeneity driven by testing and reporting biases (i.e., due to large  $\gamma$ ).

We demonstrate how the proposed model could be used to estimate the IFR of COVID-19 in Europe. Note that the main purpose of this analysis is to demonstrate the feasibility of the proposed model. As such, we keep things relatively simple. For instance, we only consider countries belonging to the EU/EEA (European Economic Area), the United Kingdom, and Switzerland, as these could be considered a reasonably homogeneous group. However, we exclude Belgium since, uniquely, the country counts all suspect deaths in nursing homes as COVID-19 deaths (Lee, 2020).

We selected  $k' = 5$  studies for which we assume there is no preferential testing. To do so, we considered all European seroprevalence studies reporting an IR estimate (along with a 95% confidence/credible interval) listed in the systematic review by Ioannidis (2020a). From these, we selected only those studies that claimed to achieve a representative or random sample from their study population.

It is important to note that the seroprevalence studies were conducted amongst populations which were particularly hard hit by infection. The result is that these populations are not necessarily representative of the overall European population. It is unclear how this

might impact our model estimates. Also, while some of the seroprevalence studies report the exact number of tests conducted ( $T$ ) and the number of confirmed cases recorded ( $CC$ ), to obtain estimates for the infection rate, there are numerous adjustments (e.g., adjusting for testing sensitivity and specificity). Rather than work with the raw  $T_k$ , and  $CC_k$  numbers published in the seroprevalence studies, we calculate effective data values for  $CC_k$  and  $T_k$  based on a binomial distribution that corresponds to the reported 95% CI for the IR. By “inverting binomial confidence intervals” in this way we are able to properly use the adjusted numbers for each of the five seroprevalence studies. This is a similar approach to the strategy employed by Kümmerer et al. (2020) who assume that the IR follows a Beta distribution with parameters chosen to match the 95% CI published in Streeck et al. (2020). In the Appendix (Section 8.4), we go over the seroprevalence study data in detail.

We obtained, national official COVID-19 statistics as reported by Our World in Data (OWID, 2020). Complete data was available for 26 countries which brings the total number of groups to  $K = 31$ . The  $CC_k$  and  $T_k$  numbers were selected as reported on May 1, 2020 (or the earliest date during the following week for which data was available). Numbers for  $D_k$  for  $k = 6, \dots, K$ , were obtained from 14 days afterwards, to allow for the known delay between the onset of symptoms and death. Note that our  $T_k$  numbers are not ideal since some countries report the number of people tested, while others report the total number of tests (which will be higher if a single person is tested several times).<sup>2</sup> Also note that, as stated in Section 2.1, the  $K$  different groups should, in principle, be entirely independent samples. This is clearly not the case with the European data (case in point: there are three different groups from within Switzerland;  $k = 2$ ,  $k = 5$ , and  $k = 30$ ).

We included several covariates about each country’s population (hospital capacity, out-

---

<sup>2</sup>see [ourworldindata.org/coronavirus-testing](https://ourworldindata.org/coronavirus-testing)

break timing, and lockdown timing) to explain variation in  $IR$  and  $IFR$ . Specifically, for the  $IR$ , we consider: (1) the number days since the country reported 10 or more confirmed infections (“Days since outbreak”) (as reported by Hale et al. (2020)); (2) the number of days between a country’s first reported infection and the imposition of social distancing measures (“Days until lockdown”) (calculated based on when the Government Response Stringency Index (GRSI) reached 20 or higher as reported in OWID (2020)); and (3) the population density (“Pop. density”) (as reported by OWID (2020) and other publicly available sources<sup>3</sup>). For the  $IFR$ , we consider: (1) the share of the population that is 70 years and older (“Prop. above 70 y.o.”) (as reported in Ioannidis (2020a) or OWID (2020)); and (2) the number of hospital beds per 1,000 people (“Hosp. beds per 1,000”)<sup>4</sup>. Tables 1 and 6 list all the data used in the analysis.

## 6.1 Using only seroprevalence studies

Using only the seroprevalence studies (i.e., only the first  $k' = 5$  studies listed in Table 1), we fit the model as described in Section 4.1 without any adjustment for covariates. (With only  $K = 5$  groups there are few degrees of freedom available for including group-level covariates). The model was fit using Stan (Carpenter et al., 2017), with 4 independent chains, each with 10,000 draws (10% burn-in, thinning of 50). Figure 2 plots, in red, the posterior estimates obtained for the  $IR_k$  and  $IFR_k$  variables (for  $k = 1, \dots, 5$ ) with 95% HPD CIs, and, in light grey, the implied uncertainty intervals for the IR and IFR from

---

<sup>3</sup>For Geneva (<https://www.bfs.admin.ch/bfs/en/home/statistics/regional-statistics/regional-portraits-key-figures/cantons/geneva.html>); for Gangelt (<https://en.wikipedia.org/wiki/Gangelt>); for Split-Dalmatia ([https://en.wikipedia.org/wiki/Split-Dalmatia\\_County](https://en.wikipedia.org/wiki/Split-Dalmatia_County)); for Zurich (<https://www.bfs.admin.ch/bfs/en/home/statistics/regional-statistics/regional-portraits-key-figures/cantons/zurich.html>).

<sup>4</sup>obtained from OWID (2020) or from [www.bfs.admin.ch](http://www.bfs.admin.ch) for Geneva and Zurich cantons.

$k$	Location	Date (MM-DD)	$T_k$	$CC_k$	$P_k$	$D_k$
1	Gangelt (Germany)	04-02	153*	27*	12597	7
2	Geneva (Switzerland)	04-23	440*	48*	506765	243
3	Luxembourg	04-26	1213*	23*	615729	92
4	Split-Dalmatia (Croatia)	04-25	937*	12*	447723	29
5	Zurich (Switzerland)	04-07	1166*	13*	1520968	127
6	Luxembourg	05-01	44895	3784	625976	103
7	Austria	05-01	264079	15424	9006400	626
8	Bulgaria	05-01	46510	1506	6948450	99
9	Croatia	05-02	37557	2085	4105268	95
10	Czech Republic	05-01	258368	7682	10708978	293
11	Denmark	05-01	266124	9158	5792203	538
12	Estonia	05-01	54439	1689	1326539	62
13	Finland	05-01	106438	4995	5540716	287
14	Germany	05-03	2773432	162496	83783930	7914
15	Greece	05-01	77251	2591	10423036	156
16	Hungary	05-01	76331	2863	9660352	442
17	Iceland	05-01	49961	1797	341250	10
18	Ireland	05-01	177097	20612	4937796	1506
19	Italy	05-01	2053425	205463	60461823	31368
20	Latvia	05-01	61120	858	1886203	19
21	Lithuania	05-01	132768	1385	2722289	54
22	Netherlands	05-03	238672	40236	17134870	5670
23	Norway	05-01	156444	7710	5421243	232
24	Poland	05-01	354628	12877	37846592	883
25	Portugal	05-01	439890	24987	10196707	1184
26	Romania	05-01	183688	12240	19237691	1046
27	Slovakia	05-01	91072	1396	5459651	27
28	Slovenia	05-01	55020	1429	2078933	103
29	Spain	05-07	1625211	222045	46754781	27940
30	Switzerland	05-01	280735	29503	8654617	1588
31	United Kingdom	05-01	996826	171253	67886017	33614

Table 1:  $*CC_k$  and  $T_k$  numbers for  $k = 1, \dots, 5$  were obtained by inverting binomial confidence intervals so as to match the reported 95% CI for the estimated IRs published in the seroprevalence studies. We assume that  $\phi_k = 1$ , for  $k = 1, \dots, 5$ , (seroprevalence studies); and that  $\phi_k$  is unknown for  $k = 5, \dots, 31$ . The date listed for each group corresponds to the date (or midpoint during the study time period) of the  $CC_k$  and  $T_k$  numbers.

$k$	Location	Prop. above 70 y.o. (%)	Hosp. beds per 1,000	Days since outbreak	Days until lockdown	Pop. density (per $km^2$ )
1	Gangelt (Germany)	14	8.00	58	32	260
2	Geneva (Switzerland)	12	4.80	54	6	2032
3	Luxembourg	10	4.51	44	8	231
4	Split-Dalmatia (Croatia)	14	5.54	50	14	100
5	Zurich (Switzerland)	12	4.10	38	6	916
6	Austria	14	7.37	61	14	107
7	Bulgaria	13	7.45	49	0	65
8	Croatia	13	5.54	57	14	74
9	Czech Republic	12	6.63	56	8	137
10	Denmark	12	2.50	57	5	137
11	Estonia	13	4.69	55	13	31
12	Finland	13	3.28	56	42	18
13	Germany	16	8.00	89	32	237
14	Greece	15	4.21	57	7	83
15	Hungary	12	7.02	51	6	108
16	Iceland	9	2.91	58	15	3
17	Ireland	9	2.96	56	11	70
18	Italy	16	3.18	69	21	206
19	Latvia	14	5.57	50	10	31
20	Lithuania	14	6.56	46	13	45
21	Luxembourg	10	4.51	49	8	231
22	Netherlands	12	3.32	62	13	509
23	Norway	11	3.60	61	13	14
24	Poland	10	6.62	53	6	124
25	Portugal	15	3.39	55	7	112
26	Romania	12	6.89	54	10	85
27	Slovakia	9	5.82	50	2	113
28	Slovenia	13	4.50	54	6	103
29	Spain	14	2.97	70	37	93
30	Switzerland	13	4.53	62	6	214
31	United Kingdom	13	2.54	67	46	273

Table 2: Covariate data for the European dataset includes: the share of the population that is 70 years and older (“Prop. above 70 y.o.”), the number of hospital beds per 1,000 people (“Hosp. beds per 1,000”), the number days since the country reported 10 or more confirmed infections (“Days since outbreak”), the number of days between a country’s first reported infection and the imposition of social distancing measures (“Days until lockdown”), and the population density (“Pop. density”).

each individual study. We also plot, in black, the posterior estimate of  $g^{-1}(\beta)$  and  $g^{-1}(\theta)$  (“Overall”). We obtain an estimate for the overall IFR of  $g^{-1}(\theta) = 0.54\%$ , 95% C.I. =  $[0.43\%, 0.67\%]$ .

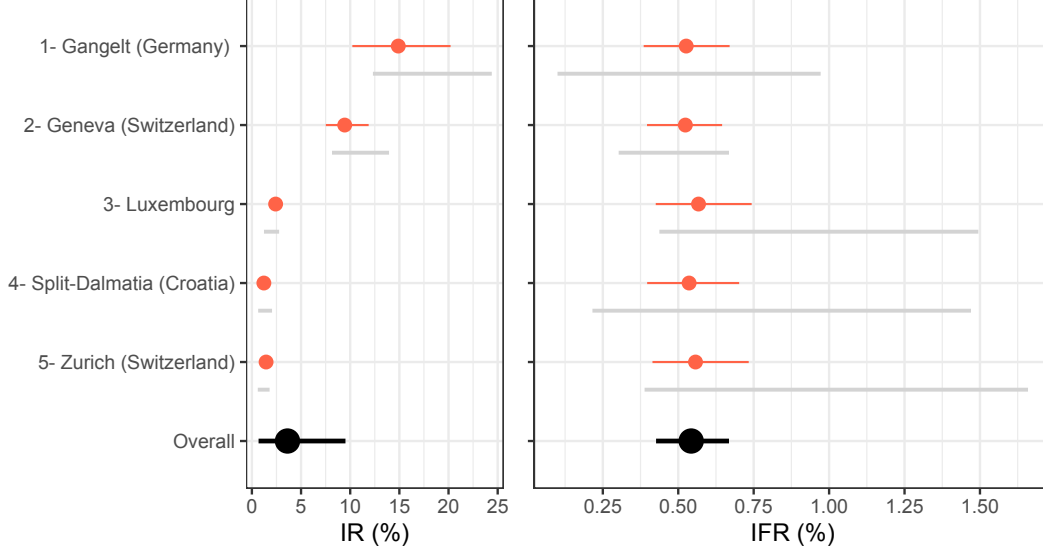


Figure 2: Posterior estimates obtained for the  $IR_k$  and  $IFR_k$  variables (for  $k = 1, \dots, 5$ ) with 95% HPD CIs. Grey lines correspond to interval estimates obtained from each seroprevalence study; red lines correspond to posterior estimates from seroprevalence studies obtained by the proposed Bayesian model pooling information across the five studies. We also plot, in black, the posterior estimate of  $g^{-1}(\beta)$  and  $g^{-1}(\theta)$  (“Overall”).

## 6.2 Using all the data

We fit the model as described in Section 4.1 to all the data (listed in Tables 1 and 6) with  $k' = 5$ ,  $K = 31$ ,  $h = 3$ , and  $q = 2$ . Covariates were defined as the centered and scaled logarithm of each metric as follows:  $X_{[1]} = \text{center-scale}(\log(\text{“Days since outbreak”}))$ ;  $X_{[2]} = \text{center-scale}(\log(\text{“Days until lockdown”} + 1))$ ;  $X_{[3]} = \text{center-scale}(\log(\text{“Population density”}))$ ;

$Z_{[1]} = \text{center-scale}(\log(\text{“Prop. above 70 y.o.”}));$  and  $Z_{[2]} = \text{center-scale}(\log(\text{“Hosp. beds per 1,000”})).$  Standard normal priors ( $\mathcal{N}(0, 1)$ ) were used for each of  $\beta_1$ ,  $\beta_2$ ,  $\beta_3$ ,  $\theta_1$ , and  $\theta_2$ . All other priors were defined as in Section 3.1 with  $\lambda = 0.5$ .

The model was fit using Stan (Carpenter et al., 2017), with 4 independent chains, each with 10,000 draws (10% burn-in, thinning of 50). Table 3 lists posterior estimates with HPD 95% CIs for the main parameters of interest. The positive value obtained for  $\theta_1$  (0.02, 95% CI = [-0.15, 0.20]) suggests that countries with older populations have higher IFRs, whereas the negative value for  $\theta_2$  (-0.44, 95% CI = [-0.63, -0.26]) suggests that countries with more hospital beds are associated with lower IFRs. The positive values for  $\beta_1$  (0.23, 95% CI = [-0.06, 0.55]) and  $\beta_2$  (0.42, 95% CI = [0.16, 0.72]) suggest that the IR increases with increasing time since the initial disease outbreak, and with increasing time between the first reported infection and the imposition of social distancing measures. Finally, the positive value for  $\beta_3$  (0.72, 95% CI = [0.44, 0.99]) suggests that a higher population density is associated with a higher IR. Note that, as with a standard multivariable regression of observational data, coefficient estimates are subject to the possibility of unobserved confounding and multicollinearity.

Figure 3 plots the posterior estimates obtained for the  $IR_k$  and  $IFR_k$  variables (for  $k = 1, \dots, 31$ ) with 95% HPD CIs. We also plot the posterior estimate of  $g^{-1}(\beta)$  and  $g^{-1}(\theta)$  (“Overall”). We obtain an estimate for overall IFR of  $g^{-1}(\theta) = 0.47\%$ , 95% C.I. = [0.34%, 0.63%]. Note that we repeated our entire analysis setting the prior for  $\gamma$  with both  $\lambda = 0.25$  and  $\lambda = 0.75$  and obtained estimates for the overall IFR of 0.50% (95% C.I. = [0.37%, 0.67%]) and of 0.44% (95% C.I. = [0.30%, 0.59%]), respectively.

Our model can no doubt be improved by using appropriately specified informed priors for the  $\phi$  parameters based on what is known about COVID-19 testing. For example, in



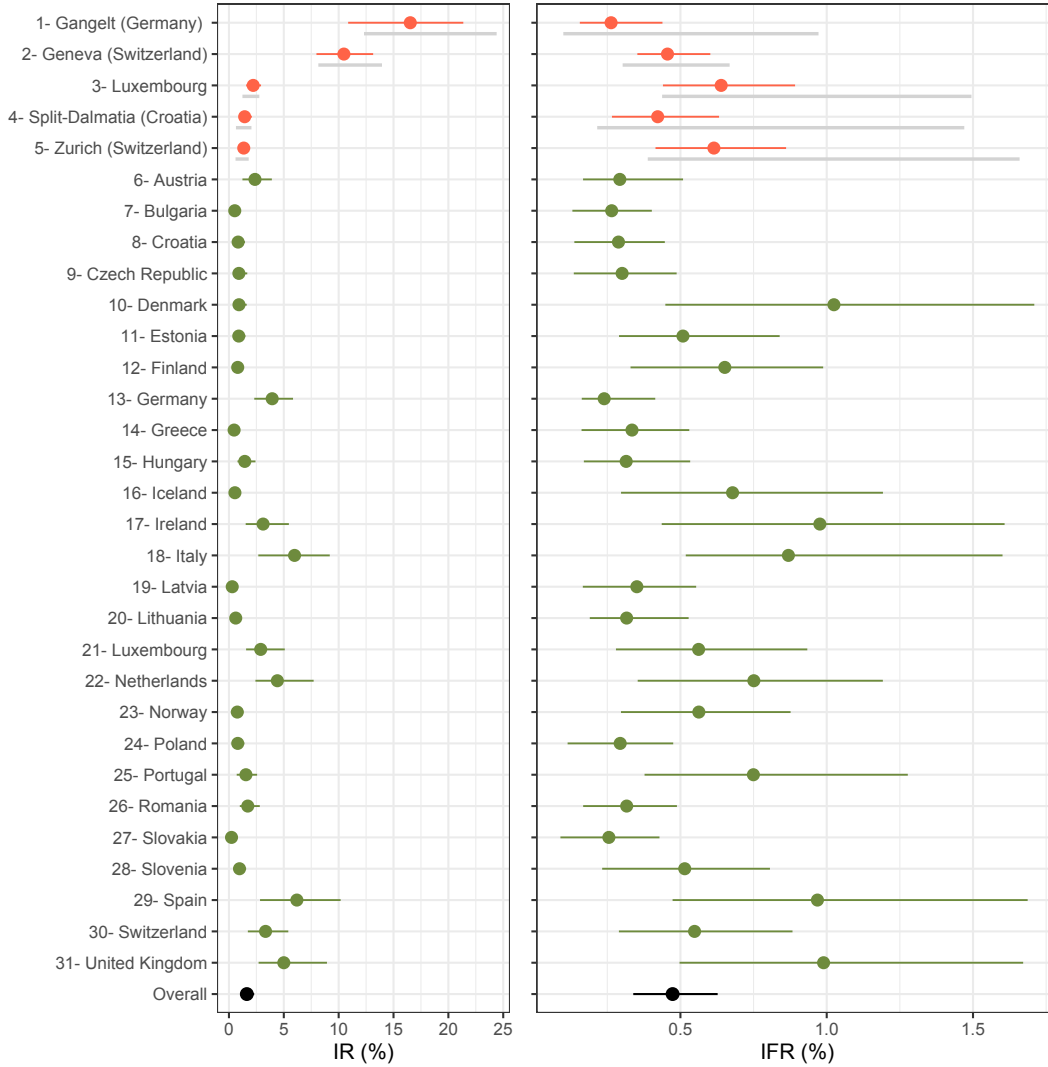


Figure 3: Posterior estimates obtained for the  $IR_k$  and  $IFR_k$  variables (for  $k = 1, \dots, 31$ ) with 95% HPD CIs. Grey lines correspond to interval estimates obtained from each seroprevalence study; red lines correspond to posterior estimates associated with populations studies in seroprevalence studies; green lines to posterior estimates corresponding to national populations. We also plot, in black, the posterior estimate of  $g^{-1}(\beta)$  and  $g^{-1}(\theta)$  (“Overall”).

	Seroprevalence data		All data	
	Estimate	95% CI	Estimate	95% CI
$g^{-1}(\theta)$	0.005	[0.004, 0.007]	0.005	[0.003, 0.006]
$g^{-1}(\beta)$	0.036	[0.007, 0.095]	0.016	[0.011, 0.023]
$\theta$	-5.213	[-5.452, -5.003]	-5.351	[-5.664, -5.054]
$\beta$	-3.300	[4.679, -2.268]	-4.108	[-4.439, -3.694]
$\theta_1$ (“Prop. above 70 y.o.”)			0.015	[-0.150, 0.195]
$\theta_2$ (“Hosp. beds per 1,000”)			-0.435	[-0.631, -0.255]
$\beta_1$ (“Days since outbreak”)			0.232	[-0.064, 0.546]
$\beta_2$ (“Days until lockdown”)			0.421	[0.156, 0.721]
$\beta_3$ (“Pop. density”)			0.720	[0.438, 0.990]
$\tau$	0.075	[0.002, 0.208]	0.251	[0.089, 0.408]
$\sigma$	1.172	[0.652, 1.94]	0.650	[0.470, 0.877]
$\gamma$			6.969	[3.148, 10.584]

Table 3: Posterior parameter estimates (posterior medians and 95% HPD CIs) from model fit to data from only the seroprevalence studies (left) and from the full dataset (right).

related work, Grewelle and De Leo (2020) assume that testing capacity is directly proportional to the case load in each country (testing capacity, is estimated by tests performed per positive case).<sup>5</sup> As another example, the “H2 index” (Hale et al., 2020), which purportedly reflects official government policy on who has access to testing within a given country, could also be used to define informed priors for the  $\phi$  parameters in a more sophisticated version of our model.

We were curious as to whether the posterior model estimates we obtained for  $\phi_k$  (for  $k = 6, \dots, 31$ ) were predictive of the H2 index. Using the data made available by Hale et al. (2020), we calculated the average H2 index for each country in our analysis, for the period between February 1st, 2020 and April 1st, 2020. Roughly speaking, a high H2 value indicates broad access to testing (i.e., available to the general public) whereas a low H2

<sup>5</sup>Grewelle and De Leo (2020) are thereby able to infer the “global IFR” using simple weighted linear regression (i.e., regressing  $\log(D_k/CC_k) \sim \log(IFR_k) + \beta_1(CC_k/T_k)$ , for  $k$  in  $1, \dots, K$ , where  $\beta_1$  is an unknown nuisance parameter).

value reflects a testing policy that restricts testing to only those who have symptoms or meet specific criteria. Thus, countries with high H2 values should, in theory, have small values of  $\phi_k$  and vice-versa. That prediction is generally supported by the results seen in Figure 4, although Iceland, Slovakia and Croatia appear to be exceptions.

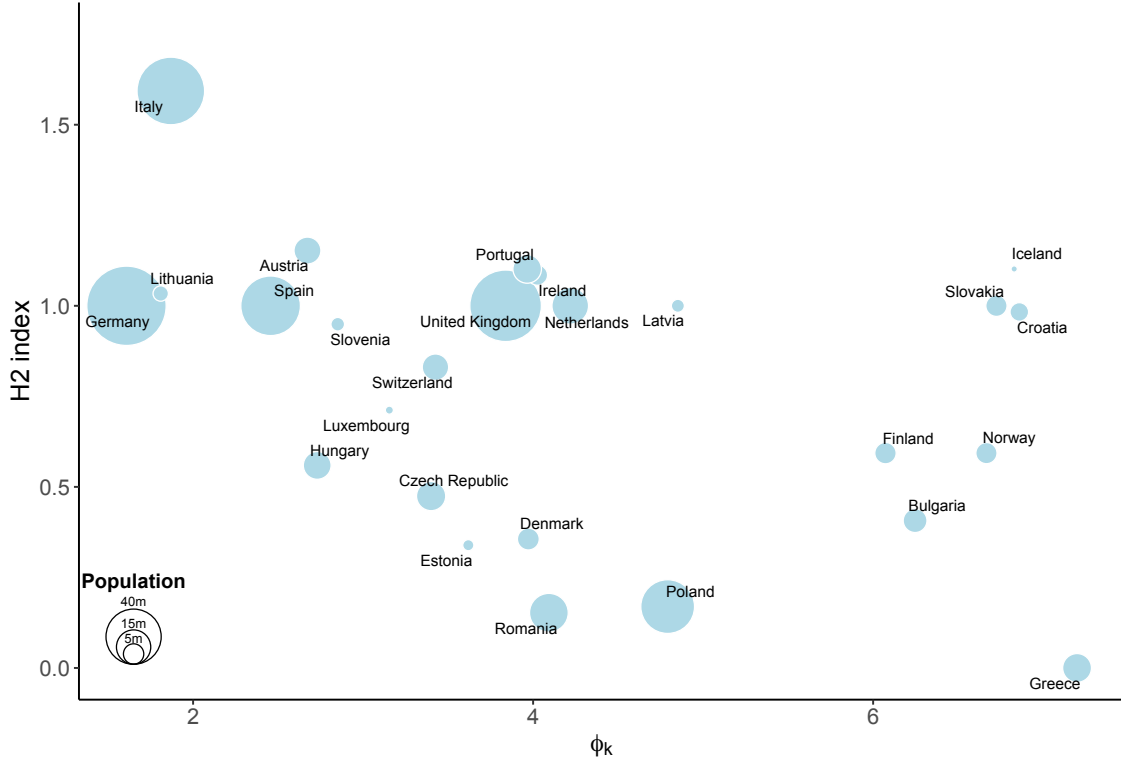


Figure 4: Scatter-plot shows of the average H2 index for each country (for the period between February 1st, 2020 and April 1st, 2020) vs. the posterior median  $\phi_k$  value. Circle size corresponds to population ( $P_k$ ).

## 7 Discussion

### 7.1 Model limitations

Estimation of the IFR is very challenging due to the fact that it is a ratio of numbers where both the numerator and denominator are subject to a wide range of biases. Our proposed model seeks to address only one particular type of bias pertaining to the denominator: the bias in the number of cases due to preferential testing. With this in mind, we wish to call attention to several other important sources of bias.

Cause of death information may be very inaccurate. To overcome this issue, many suggest looking to “excess deaths,” by comparing aggregate data for all-cause deaths from the time during the pandemic to the years prior (Leon et al., 2020). Using this approach and a simple Bayesian binomial model, Rinaldi and Paradisi (2020) are able to obtain IFR estimates without relying on official (possibly inaccurate) data for the number of COVID-19 deaths.

Some people who are currently sick and therefore at risk will eventually die of the disease, but have not died yet. Due to the delay between disease onset and death, the number of confirmed and reported COVID-19 deaths at a certain point in time will not reflect the total number of deaths that will occur among those already infected (right-censoring). This will result in the number of recorded deaths underestimating the true risk of death. The denominator of the IFR must be the number of cases *with known outcomes*.

The model, as currently proposed, fails to account for the (unknown) number of false positive and false negative tests. When both the test specificity and the infection rate is low, false positives can substantially inflate the estimated infection rate and as a consequence, the IFR could be biased downwards. In principle, the model could accommodate for this

by specifying priors for test sensitivity and specificity; see Kümmerer et al. (2020); Gelman and Carpenter (2020) and Neil et al. (2020).

Finally, because the model uses data that are aggregated at the group level, estimates are potentially subject to ecological bias (Pearce, 2000). While including group-level covariates may help reduce variability in the estimates, adjustment using group-level covariates can also lead to biased, misleading results (Li and Hua, 2020).

## 7.2 Concluding remarks

We demonstrated our proposed model with an application to European COVID-19 data, in which we relied on data from seroprevalence studies that self-reported as representative. When combined with data from nationally reported statistics, this data enabled us to obtain appropriate estimates for not only the overall IFR but also for country-level IFRs and IRs, as well as for the association of these with various explanatory factors. We note that our estimate for the overall IFR (0.47%, 95% C.I. = [0.34%, 0.63%]) is somewhat lower than an estimate obtained by the meta-analysis of Meyerowitz-Katz and Merone (2020) from European seroprevalence studies (0.77%, 95% C.I. = [0.55%, 0.99%]) and reiterate that the primary intention of our analysis was to demonstrate the feasibility of the proposed model.

Existing efforts to better understand the distribution of SARS-CoV-2 infection (and its lethality) at the population level are unfortunately met by recruiting challenges (Gudbjartsson et al., 2020; Bendavid et al., 2020), leading to an over-representation of people who are concerned about their exposure and/or an under-representation of individuals who are self-quarantining, isolating, or hospitalized because of the virus. Obtaining representative data, while challenging and costly, is however, possible. In Spain, a nationwide population-based seroprevalence study was recently completed (Pollán et al., 2020) and by combining

these data with available excess mortality data (recorded at the provincial level from the Instituto Nacional de Estadística (INE, 2020)), researchers should be able to obtain relatively unbiased and accurate estimates of the COVID-19 IFR for the Spanish population. Outside of Spain, in the absence of large-scale unbiased data, researchers must work with whatever data is available. Our model suggests a coherent way to do just this. Indeed, we demonstrated that, when fit with an appropriate model, biased data can supplement any available representative data in order to refine one’s inference and shed light on the impact of explanatory factors.

In a typical situation of drawing inference from a single biased sample, obtaining appropriate estimates is challenging, if not impossible, without some sort of external validation data. Intuition suggests that one might only be able to do a sensitivity analysis with respect to the impact of bias. Indeed, applying prior distributions for the degree of preferential testing and proceeding with Bayesian inference could be regarded as a probabilistic form of sensitivity analysis (see, for instance, Greenland (2005)). What is perhaps less intuitive, and what we demonstrated with the proposed model, is that, if one has multiple samples of biased data, each subject to a different degree of bias, the “heterogeneity of bias” can help inform what overall adjustment is required for appropriate inference.

The aggregation of data from both biased and unbiased samples is a problem that applies to many types of evidence synthesis (and is often overlooked) (De Angelis et al., 2015; Birrell et al., 2018). In that sense, the solutions we put forward may be more broadly applicable. Future work will investigate whether the “heterogeneity of bias” principle of can be used to derive appropriate estimates in a meta-analysis where individual studies are subject to varying degrees of bias due to unobserved confounding or measurement error.

# References

- Anderson, R. M., Heesterbeek, H., Klinkenberg, D., and Hollingsworth, T. D. (2020). How will country-based mitigation measures influence the course of the covid-19 epidemic? *The Lancet*, 395(10228):931–934.
- Bendavid, E., Mulaney, B., Sood, N., Shah, S., Ling, E., Bromley-Dulfano, R., Lai, C., Weissberg, Z., Saavedra, R., Tedrow, J., et al. (2020). Covid-19 antibody seroprevalence in Santa Clara County, California. *medRxiv*.
- Berger, J. O. (2013). *Statistical decision theory and Bayesian analysis*. Springer Science & Business Media.
- Birrell, P. J., De Angelis, D., and Presanis, A. M. (2018). Evidence synthesis for stochastic epidemic models. *Statistical science: a review journal of the Institute of Mathematical Statistics*, 33(1):34.
- Carpenter, B., Gelman, A., Hoffman, M. D., Lee, D., Goodrich, B., Betancourt, M., Brubaker, M., Guo, J., Li, P., and Riddell, A. (2017). Stan: A probabilistic programming language. *Journal of Statistical Software*, 76(1).
- Cochran, J. J. (2020). Why we need more coronavirus tests than we think. *Significance*.
- De Angelis, D., Presanis, A. M., Birrell, P. J., Tomba, G. S., and House, T. (2015). Four key challenges in infectious disease modelling using data from multiple sources. *Epidemics*, 10:83–87.
- De Smedt, T., Merrall, E., Macina, D., Perez-Vilar, S., Andrews, N., and Bollaerts, K. (2018). Bias due to differential and non-differential disease-and exposure misclassification in studies of vaccine effectiveness. *PloS One*, 13(6).
- de Valpine, P., Turek, D., Paciorek, C. J., Anderson-Bergman, C., Lang, D. T., and Bodik, R. (2017). Programming with models: writing statistical algorithms for general model structures with nimble. *Journal of Computational and Graphical Statistics*, 26(2):403–413.
- Emmenegger, M., De Cecco, E., Lamparter, D., Jacquat, R. P., Ebner, D., Schneider, M. M., Morales, I. C., Schneider, D., Dogancay, B., Guo, J., et al. (2020). Early plateau of sars-cov-2 seroprevalence identified by tripartite immunoassay in a large population. *medRxiv*.

- Faust, J. S. (2020). Comparing covid-19 deaths to flu deaths is like comparing apples to oranges. *Scientific American*, <https://tinyurl.com/ydxx8e18>.
- Fog, A. (2008). Sampling methods for Wallenius’ and Fisher’s noncentral hypergeometric distributions. *Communications in Statistics Simulation and Computation*, 37(2):241–257.
- Gelman, A. and Carpenter, B. (2020). Bayesian analysis of tests with unknown specificity and sensitivity. <https://tinyurl.com/ybgunxsk>.
- Greenland, S. (2005). Multiple-bias modelling for analysis of observational data. *Journal of the Royal Statistical Society: Series A (Statistics in Society)*, 168(2):267–306.
- Grewelle, R. and De Leo, G. (2020). Estimating the global infection fatality rate of covid-19. *medRxiv*.
- Gudbjartsson, D. F., Helgason, A., Jonsson, H., Magnusson, O. T., Melsted, P., Norddahl, G. L., Saemundsdottir, J., Sigurdsson, A., Sulem, P., Agustsdottir, A. B., et al. (2020). Spread of sars-cov-2 in the icelandic population. *New England Journal of Medicine*.
- Gustafson, P. (2010). Bayesian inference for partially identified models. *The International Journal of Biostatistics*, 6(2).
- Gustafson, P., Greenland, S., et al. (2009). Interval estimation for messy observational data. *Statistical Science*, 24(3):328–342.
- Hale, T., Webster, S., Petherick, A., Phillips, T., and Kira, B. (2020). Oxford covid-19 government response tracker. <https://www.bsg.ox.ac.uk/research/research-projects/coronavirus-government-response-tracker#data>.
- Hauser, A., Counotte, M. J., Margossian, C. C., Konstantinoudis, G., Low, N., Althaus, C. L., and Riou, J. (2020). Estimation of sars-cov-2 mortality during the early stages of an epidemic: a modelling study in Hubei, China and northern Italy. *medRxiv*.
- INE (2020). Estimación del número de defunciones semanales durante el brote de covid-19. [https://www.ine.es/experimental/defunciones/experimental\\_defunciones.htm](https://www.ine.es/experimental/defunciones/experimental_defunciones.htm).
- Ioannidis, J. (2020a). The infection fatality rate of covid-19 inferred from seroprevalence data (version 2 (June 8, 2020 - 14:00)). *medRxiv*.



- Ioannidis, J. P. (2020b). First Opinion: A fiasco in the making? as the coronavirus pandemic takes hold, we are making decisions without reliable data. STAT, <https://tinyurl.com/uj539o4>.
- Jerkovic, I., Ljubic, T., Basic, Z., Kruzic, I., Kunac, N., Bezic, J., Vuko, A., Markotic, A., and Andjelinovic, S. (2020). Sars-cov-2 antibody seroprevalence in industry workers in split-dalmatia and sibenik-knin county, croatia. *medRxiv*.
- Kobayashi, T., Jung, S.-m., Linton, N. M., Kinoshita, R., Hayashi, K., Miyama, T., Anzai, A., Yang, Y., Yuan, B., Akhmetzhanov, A. R., et al. (2020). Communicating the risk of death from novel coronavirus disease (covid-19).
- Kruschke, J. (2014). *Doing Bayesian data analysis: A tutorial with R, JAGS, and Stan*. Academic Press.
- Kümmerer, M., Berens, P., and Macke, J. (2020). A simple bayesian analysis of the infection fatality rate in gangelt, and an uncertainty aware extrapolation to infection-counts in Germany. <https://matthias-k.github.io/BayesianHeinsberg.html>.
- Lambert, P. C., Sutton, A. J., Burton, P. R., Abrams, K. R., and Jones, D. R. (2005). How vague is vague? A simulation study of the impact of the use of vague prior distributions in mcmc using winbugs. *Statistics in Medicine*, 24(15):2401–2428.
- Lee, G. (2020). Coronavirus: Why so many people are dying in Belgium. *BBC.com*, <https://www.bbc.com/news/world-europe-52491210>.
- Leon, D. A., Shkolnikov, V. M., Smeeth, L., Magnus, P., Pechholdová, M., and Jarvis, C. I. (2020). Covid-19: a need for real-time monitoring of weekly excess deaths. *The Lancet*.
- Li, S. and Hua, X. (2020). The closer to the Europe Union headquarters, the higher risk of covid-19? Cautions regarding ecological studies of covid-19. *medRxiv*.
- Lipsitch, M. (2020). First Opinion: We know enough now to act decisively against covid-19. social distancing is a good place to start. STAT, <https://tinyurl.com/yx4gf9mr>.
- Manski, C. F. (2003). *Partial identification of probability distributions*. Springer Science & Business Media.
- Meyerowitz-Katz, G. and Merone, L. (2020). A systematic review and meta-analysis of published research data on covid-19 infection-fatality rates (version 4). *medRxiv*.

- Morris, T. P., White, I. R., and Crowther, M. J. (2019). Using simulation studies to evaluate statistical methods. *Statistics in Medicine*, 38(11):2074–2102.
- Neil, M., Fenton, N., Osman, M., and McLachlan, S. (2020). Bayesian network analysis of covid-19 data reveals higher infection prevalence rates and lower fatality rates than widely reported. *medRxiv*.
- Onder, G., Rezza, G., and Brusaferro, S. (2020). Case-fatality rate and characteristics of patients dying in relation to covid-19 in Italy. *JAMA*.
- OWID, O. W. I. D. (2020). Codebook for the complete our world in data covid-19 dataset. <https://github.com/owid/covid-19-data/blob/master/public/data/owid-covid-data-codebook.md>.
- Pearce, N. (2000). The ecological fallacy strikes back. *Journal of Epidemiology & Community Health*, 54(5):326–327.
- Pellis, L., Cauchemez, S., Ferguson, N. M., and Fraser, C. (2020). Systematic selection between age and household structure for models aimed at emerging epidemic predictions. *Nature Communications*, 11(1):1–11.
- Perez-Saez, J., Lauer, S. A., Kaiser, L., Regard, S., Delaporte, E., Guessous, I., Stringhini, S., Azman, A. S., Group, S.-P. S., et al. (2020). Serology-informed estimates of sars-cov-2 infection fatality risk in Geneva, Switzerland. *medRxiv*.
- Pollán, M., Pérez-Gómez, B., Pastor-Barriuso, R., Oteo, J., Hernán, M. A., Pérez-Olmeda, M., Sanmartín, J. L., Fernández-García, A., Cruz, I., de Larrea, N. F., et al. (2020). Prevalence of sars-cov-2 in spain (ene-covid): a nationwide, population-based seroepidemiological study. *The Lancet*.
- Presanis, A. M., De Angelis, D., Flu, T. N. Y. C. S., Team, I., Hagy, A., Reed, C., Riley, S., Cooper, B. S., Finelli, L., Biedrzycki, P., et al. (2009). The severity of pandemic H1N1 influenza in the united states, from April to July 2009: a Bayesian analysis. *PLoS Medicine*, 6(12).
- Prochaska, C. and Theodore, L. (2018). Discrete probability distributions. *Introduction to Mathematical Methods for Environmental Engineers and Scientists*, page 287.
- Rinaldi, G. and Paradisi, M. (2020). An empirical estimate of the infection fatality rate of covid-19 from the first Italian outbreak. *medRxiv*.

- Sahai, H. and Khurshid, A. (1995). *Statistics in epidemiology: methods, techniques and applications*. CRC press.
- Snoeck, C. J., Vaillant, M., Abdelrahman, T., Satagopam, V. P., Turner, J. D., Beaumont, K., Gomes, C. P., Fritz, J. V., Schröder, V. E., Kaysen, A., et al. (2020). Prevalence of sars-cov-2 infection in the luxembourgish population: the CON-VINCE study. *medRxiv*.
- Stevens, W. (1951). Mean and variance of an entry in a contingency table. *Biometrika*, 38(3/4):468–470.
- Streeck, H., Schulte, B., Kuemmerer, B., Richter, E., Höller, T., Fuhrmann, C., Bartok, E., Dolscheid, R., Berger, M., Wessendorf, L., et al. (2020). Infection fatality rate of sars-cov-2 infection in a german community with a super-spreading event. *medRxiv*.
- Stringhini, S., Wisniak, A., Piumatti, G., Azman, A. S., Lauer, S. A., Baysson, H., De Ridder, D., Petrovic, D., Schrempt, S., Marcus, K., et al. (2020). Seroprevalence of anti-sars-cov-2 igg antibodies in Geneva, Switzerland (serocov-pop): a population-based study. *The Lancet*.
- Wong, J. Y., Heath Kelly, D. K., Wu, J. T., Leung, G. M., and Cowling, B. J. (2013). Case fatality risk of influenza A (H1N1pdm09): a systematic review. *Epidemiology (Cambridge, Mass.)*, 24(6).

## SUPPLEMENTARY MATERIAL

### 8 Appendix

#### 8.1 Issues of (un)identifiability

Table 4 provides a small artificial dataset to help illustrate the type of data being described and the impact of different degrees of preferential testing. In this dataset, we have  $K = 12$  groups and the (unknown) infection rate varies substantially from 13% to 53%. The unknown infection fatality rate only varies slightly, from 0.017% to 0.022%. Values for  $\phi_k$  in this dataset are evenly distributed between 1 and  $\gamma + 1$ , for four different values of  $\gamma = 0, 4, 11$ , and 22. When  $\gamma = 0$ , the number of true cases (i.e. actual infections) is approximately 14 times higher than the number of confirmed cases. In contrast, when  $\gamma = 22$ , the number of true cases is only about 5 times higher than the number of confirmed cases.

	Observed,				$\gamma = 0$				Unobserved,				$\gamma = 4$			
$k$	$P_k$	$T_k$	$D_k$	$CC_k$	$CC_k$	$CC_k$	$CC_k$	$C_k$	$IR_k$	$IFR_k$	$\phi_k$	$\phi_k$	$\phi_k$			
1	3061	190	11	24	21	32	27	430	0.140	0.018	1	1	1			
2	482	43	2	15	11	12	24	99	0.206	0.020	1.36	2	3			
3	1882	101	20	32	40	55	74	570	0.303	0.022	1.73	3	5			
4	1016	67	2	14	24	33	38	193	0.190	0.017	2.09	4	7			
5	1269	109	4	13	34	54	67	201	0.159	0.021	2.45	5	9			
6	3670	276	9	53	70	140	162	484	0.132	0.021	2.82	6	11			
7	2409	139	7	17	34	70	94	329	0.137	0.019	3.18	7	13			
8	1074	81	13	42	65	68	77	565	0.526	0.019	3.55	8	15			
9	3868	289	16	60	142	205	247	821	0.212	0.019	3.91	9	17			
10	151	13	2	1	5	11	8	24	0.160	0.019	4.27	10	19			
11	430	25	1	6	9	16	18	70	0.164	0.019	4.64	11	21			
12	429	40	2	11	23	31	33	105	0.245	0.019	5	12	23			

Table 4: Illustrative Example Data, with varying degrees of preferential sampling,  $\gamma = 0$ ,  $\gamma = 4$ ,  $\gamma = 11$ , and  $\gamma = 22$ .

Here we present an asymptotic argument which lays bare the flow of information. Consider a situation in which an infinite amount data are available. In so-called “asymptotia,” we have that populations are approaching infinite size (i.e., for  $k$  in  $1, \dots, K$ , we have  $P_k \rightarrow \infty$ ), and that the number of tests also approaches infinity (i.e., for  $k$  in  $1, \dots, K$ , we have  $T_k \rightarrow \infty$ ). Recall that a hyper-geometric distribution is asymptotically equivalent to a binomial distribution. As such, we consider the following:

$$D_k \sim \text{Binom}(P_k, a_k); \text{ and}$$

$$CC_k \sim \text{Binom}(T_k, b_k),$$

where  $a_k = IFR_k \times IR_k$  and  $b_k = 1 - (1 - IR_k)^{\phi_k}$ .

Note that  $a_k$  simply follows from the conditional binomial distribution. However, this particular parameterization of  $b_k$  does not emerge from the limit of the non-central hyper-geometric distribution. As we discuss later in Section 4.1, we have simply chosen a convenient parameterization for  $b_k$  with the important connotation that  $\phi_k = 1$  corresponds to testing at random, but as  $\phi_k$  increases, the testing is more preferentially weighted to those truly infected. For example, with an infection rate of  $IR_k = 0.01$ , the binomial sampling probability,  $b_k$ , is approximately 10 times larger than the infection rate if  $\phi_k = 10$ , and about 18 times larger if  $\phi_k = 20$ .

Presume that the *a priori* defensible information about the preferential sampling in the  $k$ -th group is expressed in the form

$$\phi_k \in [\underline{\phi}_k, \bar{\phi}_k], \tag{13}$$

i.e.,  $\underline{\phi}_k$  and  $\bar{\phi}_k$  are investigator-specified bounds on the degree of preferential sampling for that jurisdiction. If one is certain that cases are as likely, or at least as likely, to be tested as non-cases,  $\underline{\phi}_k = 1$  is appropriate. If testing is known to be entirely random for the  $k$ -th

group, one would set  $\phi_k = \bar{\phi}_k = 1$ .

Note that for fixed  $(a_k, b_k)$ ,  $IFR_k$  is a function of  $\phi_k$  with the form

$$IFR_k(\phi_k) = \frac{a_k}{1 - (1 - b_k)^{(1/\phi_k)}}. \quad (14)$$

Examining (14), knowledge of  $(a_k, b_k)$ , in tandem with (13) restricts the set of possible values for  $IFR_k$ . In fact it is easy to verify that (14) is monotone in  $\phi_k$ , hence the restricted set is an interval. We write this interval as  $I_k(a_k, b_k, \phi_k, \bar{\phi}_k)$ , or simply as  $I_k$  for brevity. This is the jurisdiction-specific *identification interval* for  $IFR_k$ . As we approach asymptotia for the  $k$ -th group, all values inside the interval remain plausible, while all values outside are ruled out; see Manski (2003). This is the essence of the *partial identification* inherent to this problem.

Thinking now about the meta-analytic task of combining information, we envision that both  $\phi_k$  and  $IFR_k$  could exhibit considerable variation across jurisdictions. However, the variation in  $IFR$  could be small, particularly if sufficient jurisdiction-specific covariates are included (see Section 4.2). That is, after adjustment for a jurisdiction's age-distribution, healthcare capacity, and so on, residual variation in  $IFR$  could be very modest. When modeling, we would invoke such an assumption via a prior distribution. For understanding in asymptotia, however, we simply consider the impact of an *a priori* bound on the variability in  $IFR$ . Let  $\tau$  be the standard deviation of  $IFR$  across jurisdictions. Then we presume  $\tau$  does not exceed an investigator-specified upper bound of  $\bar{\tau}$ , i.e.,  $\tau \leq \bar{\tau}$ .

The jurisdiction-specific prior bounds on the extent of preferential sampling, and the prior bound on  $IFR$  variation across jurisdictions, along with the limiting signal from the data in the form of  $(a, b)$ , gives rise to an identification region for the average infection

fatality rate,  $\overline{IFR} = K^{-1} \sum_{k=1}^K IFR_k$ . Formally, this interval is defined as

$$I(a, b, \underline{\phi}, \bar{\phi}, \bar{\tau}) = \{ \overline{IFR} : \tau \leq \bar{\tau}, IFR_k \in I_k(a_k, b_k, \underline{\phi}_k, \bar{\phi}_k), \forall k \in \{1, \dots, K\} \}. \quad (15)$$

Again, the interpretation is direct: in the asymptotic limit, all values of  $\overline{IFR}$  inside this interval are compatible with the observed data, and all values outside are not. The primary question of interest is whether this interval is narrow or wide under realistic scenarios, since this governs the extent to which we can learn about  $\overline{IFR}$  from the data.

In general, evaluating (15) for given inputs is an exercise in quadratic programming nested within a grid search, hence can be handled with standard numerical optimisation. However, the special case of  $\bar{\tau} = 0$  is noteworthy in terms of developing both scientific and mathematical intuition. Consequently, we explore this case in some depth in what follows.

Scientifically,  $\bar{\tau} = 0$  represents the extreme limit of an *a priori* assumption that, possibly after covariate adjustment,  $IFR$  is a ‘biological constant’ which does not vary across jurisdictions. If the prospects for inference are not good when this assumption holds, they will be even less good under the less strict assumption that the  $IFR$  heterogeneity is small, but not necessarily zero. Mathematically, the case is much simpler, with (15) reducing to

$$I(a, b, \underline{\phi}, \bar{\phi}, 0) = \cap_k I_k(a_k, b_k, \underline{\phi}_k, \bar{\phi}_k). \quad (16)$$

As intuition must have it, without heterogeneity, a putative value for the ‘global’ IFR is compatible with the observed data if and only if it is compatible with the data from *every* jurisdiction individually.

To illustrate, consider a scenario with  $K = 12$  jurisdictions, with a constant infection fatality rate of 2%, i.e.,  $IFR_k = 0.02$ , for  $k$  in  $1, \dots, 12$ . Say that the infection rates for

these jurisdictions lie between 0.132 and 0.526, as per Table 1. Furthermore, say that the unknown  $\phi_k$  values range between 1 and 23, as per the rightmost column ( $\gamma = 22$ ) of Table 1.

Now say the investigator pre-specifies  $(\phi_k, \bar{\phi}_k) = (1, 40)$  for all  $k$ . As such, the *a priori* bounds are correct, for all jurisdictions. The resulting jurisdiction-specific identification intervals,  $I_k$ , are depicted in the bottom left-hand panel of Figure 5. (The top and middle left-hand panels correspond to the identical situation but with  $\phi_k$  values listed in the  $\gamma = 4$  and  $\gamma = 11$  columns of Table 1 respectively.) Also depicted by the green rectangle is the global identification interval, i.e., the intersection of the individual intervals. In the present scenario ( $\gamma = 22$ ), this is indeed narrow, ranging from 0.0200 to 0.0328. (For the  $\gamma = 4$ ,  $\gamma = 11$  and  $\gamma = 22$  scenarios, the global identification intervals are  $[0.0200, 0.1419]$ ,  $[0.0200, 0.0606]$ , and  $[0.0200, 0.0328]$ , respectively.) Thus, depending on the range and heterogeneity in  $\phi_k$  values, it appears that data can contribute substantial information about the (constant) infection fatality rate.

As can be seen immediately from Figure 5 (left-hand panels), in the present example the binding constraints arise from the first and twelfth jurisdictions, which happen to have the least and most amounts of preferential testing. However, this pattern does not hold in general. One can easily construct pairs of infection rates for which the jurisdiction with more preferential testing has a smaller upper endpoint for  $I_k$  and/or a larger lower endpoint. Thus the values of  $\phi_k$  alone do not determine which two jurisdictions will provide the binding information about  $\overline{IFR}$ .

Figure 5 (right-hand panels) shows how the global identification interval is wider when  $\bar{\tau} = 0.002$ . For reference, for the IFR values listed in Table 1,  $\tau = SD(IFR_{1:12}) = 0.00124$ . For the  $\gamma = 4$ ,  $\gamma = 11$ , and  $\gamma = 22$  scenarios, the global identification intervals outlined by



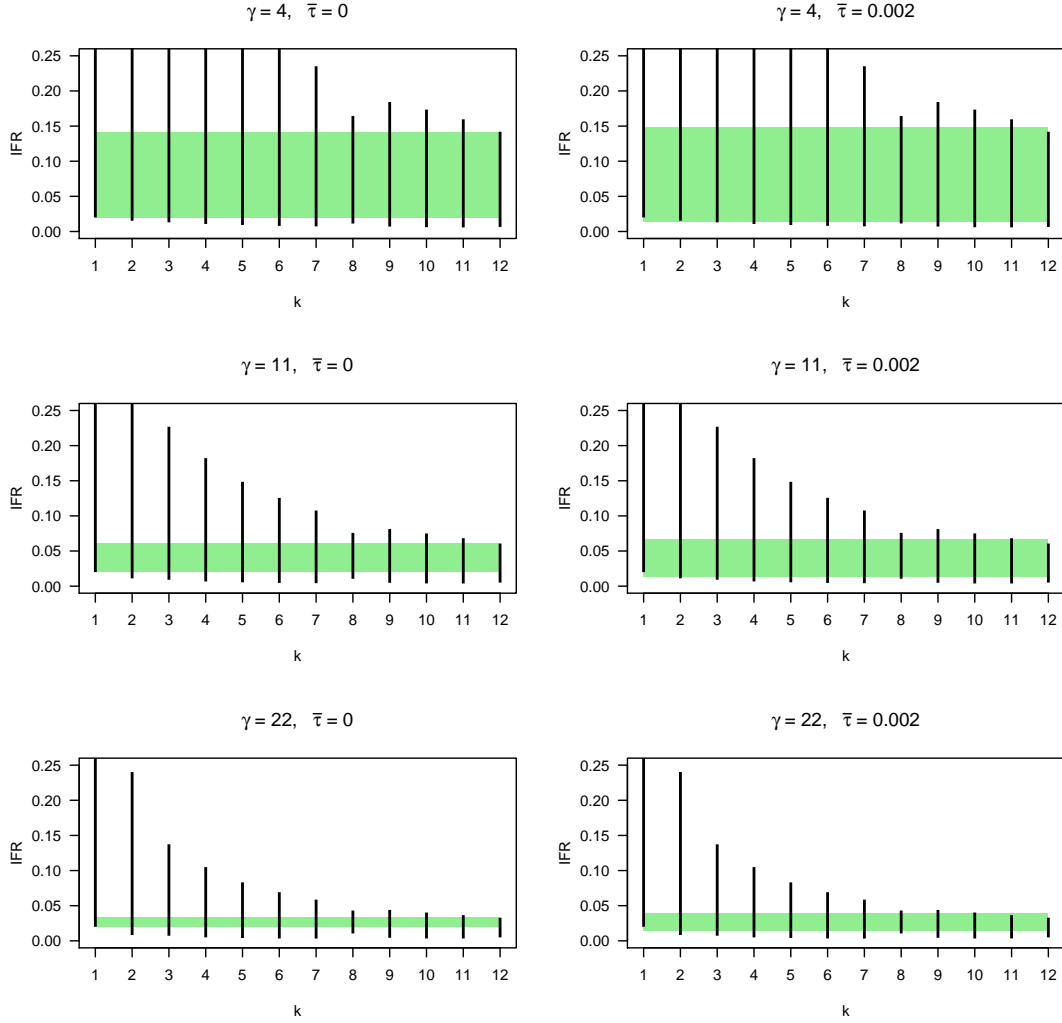


Figure 5: Black lines correspond to jurisdiction-specific identification intervals and the green rectangle corresponds to the global identification interval. Left-hand panels correspond to assumption of  $\bar{\tau} = 0$  such the global identification interval is simply the intersection of the individual intervals. Right-hand panels correspond to  $\bar{\tau} = 0.002$ .

the green rectangles are  $[0.0139, 0.1483]$ ,  $[0.0137, 0.0670]$  and  $[0.0137, 0.0386]$ , respectively.

Now consider the evaluation of (15) for  $\bar{\tau} > 0$ , i.e., where a limited heterogeneity in  $IFR$  is permitted. Recall that quadratic programming constitutes the minimization of a quadratic function subject to linear constraints, and these may be a mix of equality and inequality constraints. Let  $x$  be a candidate value, which we will test for membership in the identification interval. To perform this test, we use a standard quadratic programming package (quadprog) to minimize the quadratic function  $Var(IFR)$ , subject to the equality constraint  $\overline{IFR} = x$  and the  $2K$  inequality constraints which restrict  $IFR_k$  to the interval  $I_k$  for each  $k$ . By the definition of (6) then,  $x$  belongs in the identification interval if and only if the minimized variance does not exceed  $\bar{\tau}^2$ .

Thus a simple grid search over values of  $x$  numerically determines the identification interval. Note that so long as  $a$  and  $b$  arise from values of  $\phi$  within the prescribed bounds, the underlying value of  $\overline{IFR}$  must belong to the identification interval. Thus two numerical searches can be undertaken. One starts at the underlying value and tests successively larger  $x$  until a failing value is obtained. The other starts at the underlying value and does the same, but moving downwards.

## 8.2 Illustrative example

We illustrate the proposed model with the simple artificial dataset introduced earlier in Table 4. The dataset considers  $K = 12$  groups with average populations of 2,000 individuals ( $P_k$  obtained from a  $NegBin(2000, 1)$  distribution). The data were simulated such that, across all 12 groups, the expected overall IFR is 2% (i.e.,  $icloglog(\theta) = 0.02$ ;  $\theta = -3.90$ ), and the expected overall IR is 20% (i.e.,  $icloglog(\beta) = 0.20$ ;  $\beta = -1.50$ ). Variability between populations was allowed by selecting  $\tau^2 = 0.005$  and  $\sigma^2 = 0.25$ . The testing

rate for each population was obtained from a  $Uniform(0.01, 0.10)$  distribution so that the number of tests in each population ranged from 1% of individuals to 10%.

		Truth	$M_1$			$M_{\{\gamma=0\}}$		
			2.5%	50%	97.5%	2.5%	50%	97.5%
$\gamma = 0$	$g^{-1}(\theta)$	0.020	0.019	0.030	0.054	0.017	0.022	0.027
	$g^{-1}(\beta)$	0.200	0.081	0.158	0.264	0.157	0.218	0.301
	$\tau$	0.071	0.000	0.067	0.192	0.000	0.069	0.194
	$\sigma$	0.50	0.304	0.546	0.898	0.313	0.547	0.869
	$\gamma$	0	0.000	1.140	4.531			
$\gamma = 4$	$g^{-1}(\theta)$	0.020	0.013	0.023	0.039	0.011	0.013	0.017
	$g^{-1}(\beta)$	0.200	0.109	0.207	0.382	0.253	0.361	0.490
	$\tau$	0.071	0.000	0.076	0.213	0.000	0.113	0.255
	$\sigma$	0.50	0.365	0.641	1.024	0.397	0.652	1.018
	$\gamma$	4	0.002	3.337	8.549			
$\gamma = 11$	$g^{-1}(\theta)$	0.020	0.010	0.017	0.026	0.007	0.009	0.011
	$g^{-1}(\beta)$	0.200	0.171	0.292	0.490	0.413	0.550	0.699
	$\tau$	0.071	0.000	0.083	0.228	0.000	0.174	0.310
	$\sigma$	0.50	0.329	0.626	1.038	0.397	0.653	1.024
	$\gamma$	11	0.855	5.972	12.697			
$\gamma = 22$	$g^{-1}(\theta)$	0.020	0.008	0.013	0.020	0.006	0.007	0.010
	$g^{-1}(\beta)$	0.200	0.216	0.365	0.592	0.495	0.648	0.799
	$\tau$	0.071	0.000	0.098	0.249	0.000	0.187	0.323
	$\sigma$	0.50	0.404	0.685	1.103	0.432	0.701	1.078
	$\gamma$	22	1.109	6.966	14.806			

Table 5: Illustrative Example Data - Posterior medians and 95% HPD credible intervals.

We fit the model ( $M_1$ ) as detailed in Section 3.1, where  $k' = 0$ , and  $K = 12$ , and also fit the model where  $\gamma = 0$  is fixed ( $M_{\{\gamma=0\}}$ ), corresponding to a situation in which one assumes that none of the populations are subject to any preferential testing. Each model is fit using JAGS (just another Gibbs' sampler) (Kruschke, 2014), with 5 independent chains, each with 500,000 draws (20% burn-in, thinning of 50). The results, including posterior medians and highest posterior density (HPD) 95% credible intervals (CI), are listed in Table 5. Figures 6 - 7 plot a selection of diagnostics for the MCMC; the prior-posterior

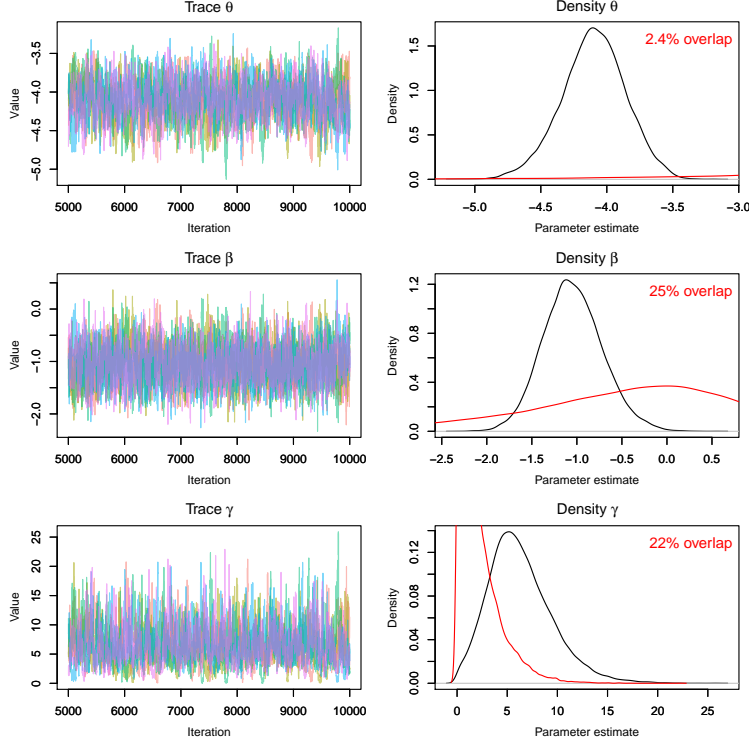


Figure 6: A selection of diagnostic plots for the MCMC simulation of the model with  $\gamma = 11$ . The left panels report trace plots from the posterior to check convergence. The right panels report the corresponding posterior distribution estimate (black solid line) together with the prior distribution for that parameter (red solid line). The % overlap reported in red is the PPO (prior-posterior overlap).

overlap numbers suggest that the data carry substantial information content about the  $\phi$  variables.

When  $\gamma = 0$ , note that the 95% CI for  $g^{-1}(\theta)$  is much wider with  $M_1$  compared to with  $M_{\{\gamma=0\}}$ . This reflects the additional uncertainty of not knowing about the absence/presence of preferential testing. Otherwise, when  $\gamma > 0$ , we see that ignoring preferential testing has significant consequences. With the  $M_{\{\gamma=0\}}$  model, the 95% CI for  $g^{-1}(\theta)$  fails to include

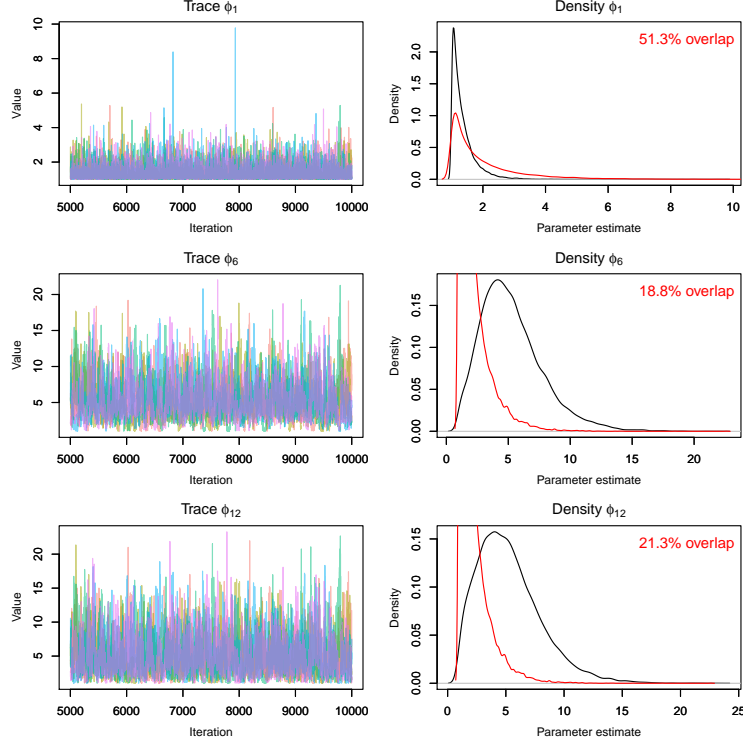


Figure 7: A selection of diagnostic plots for the MCMC simulation of the model with  $\gamma = 11$ . The left panels report trace plots from the posterior to check convergence. The right panels report the corresponding posterior distribution estimate (black solid line) together with the prior distribution for that parameter (red solid line). The % overlap reported in red is the PPO (prior-posterior overlap).

the target when  $\gamma > 0$ . When  $\gamma = 22$ , the  $M_1$  model also fails to include the target within the 95% CI for  $g^{-1}(\theta)$ . This suggests that, with limited data, there is an upper bound on the degree of preferential testing for which the model can adjust.

### 8.3 nimble MCMC details

Using nimble, we applied two sampling strategies for the trio  $(\phi_k, \text{cloglog}(\text{IR}_k), \text{cloglog}(\text{IFR}_k))$  for each  $k$  in  $1, \dots, K$ . In all cases the univariate sampling method was adaptive random-walk Metropolis-Hastings. For notation, we drop the subscript  $k$  and define  $\eta_1 = \text{cloglog}(\text{IR}_k)$  and  $\eta_2 = \text{cloglog}(\text{IFR}_k)$ .

First, we included a block sampler on  $(\phi, \eta_1, \eta_2)$  for each  $k$ , along with the usual univariate samplers on each element of the trio. Second, we included samplers in two transformed coordinate spaces. Define transformed coordinates  $(z_1, z_2) = (h_1(\eta_1, \eta_2), h_2(\eta_1, \eta_2)) = (\exp(\eta_1) + \exp(\eta_2), \exp(\eta_1) - \exp(\eta_2))$ . (Based on the cloglog link, the quantities  $\exp(\eta_1)$  and  $\exp(\eta_2)$  may be interpreted as continuous time rates.)

Now  $z_1$  represents the more strongly identified quantity, so mixing in  $z_2$  can be slow. Hence we wish to improve mixing in the  $z_2$  direction. To do so, a sampler can operate in the  $(z_1, z_2)$  coordinates while transforming the prior such that it is equivalent in  $(z_1, z_2)$  to what was specified in the original coordinates,  $(\eta_1, \eta_2)$ . Using  $P(\cdot)$  for priors, we have  $\log(P(z_1, z_2)) = \log(P(\eta_1, \eta_2)) - \log(|J|)$ , where  $|J|$  is the determinant of the Jacobian of  $(z_1, z_2)$  with respect to  $(\eta_1, \eta_2)$ . In this case,  $|J| = 2 \exp(\eta_1 + \eta_2)$ .

The other transformed coordinates used were  $(z_1, z_2) = (\log(\phi) + \eta_1, \log(\phi) - \eta_1)$ . Note that  $\log(\phi) + \eta_1 = \log(-\log((1 - \text{IR})^\phi))$ . Hence  $z_1$  represents the more strongly identified quantity, so we wish to improve mixing by sampling in the  $z_2$  direction. We have the same formulation as above, with  $|J| = 2/\phi$ .

### 8.4 Seroprevalence study data

Consider the Europe data, for  $k = 1, \dots, 5$ :

- **$k = 1$ : Gangelt, Germany-** Streeck et al. (2020) estimated the infection prevalence from a “random population sample” obtained between March 31st, 2020 and April 6th, and provide a 95% CI for the IR of [12.31%, 24.40%].<sup>6</sup> This uncertainty interval is equivalent to a binomial distribution with 27 confirmed cases from 153 tests. The relevant number of deaths is 7 (recorded on April 15th, 2020), as listed by Ioannidis (2020a). With a total population of 12,597, this corresponds to a crude frequentist 95% CI for the IFR of [0.10%, 0.97%].
- **$k = 2$ : Geneva, Switzerland-** Based on the data collected by Stringhini et al. (2020), Perez-Saez et al. (2020) estimate a 95% CI for the IR of [8.15%, 13.95%] for a “representative sample of the general population” of the canton of Geneva (enrolment between April 6th and May 9th).<sup>7</sup> This uncertainty interval is equivalent to a binomial distribution with 48 confirmed cases amongst 440 tests. The relevant number of deaths is 243 (recorded on April 30th, 2020), as listed by Ioannidis (2020a).<sup>8</sup> With a total population of 506,765, this corresponds to a crude frequentist 95% CI for the IFR of [0.30%, 0.67%].
- **$k = 3$ : Luxembourg:** Snoeck et al. (2020) “recruited a representative sample of the Luxembourgish population” between April 16th and May 5th, and obtained a 95% CI of [1.23%, 2.77%].<sup>9</sup> This uncertainty interval corresponds to about 23 confirmed cases

---

<sup>6</sup>Streeck et al. (2020) reports two different 95% CIs, obtained with an without applying a “correction factor”: [15.84%; 24.40%] and [12.31%; 18.96%], respectively.

<sup>7</sup>Population number for the canton of Geneva obtained from Perez-Saez et al. (2020).

<sup>8</sup>Ioannidis (2020a): “For the number of COVID-19 deaths, the number of deaths recorded at the time chosen by the authors of each study was selected, whenever the authors used such a death count up to a specific date to make inferences themselves. If the choice of date had not been done by the authors, the number of deaths accumulated until after 1 week of the mid-point of the study period was chosen.”

<sup>9</sup>Snoeck et al. (2020) report two different 95% CIs, obtained with an without adjustment for age, gender and canton: [1.23%; 2.67%] and [1.34%; 2.77%].

from 1,213 tests. The relevant number of deaths is 92 (recorded on May 2nd, 2020), as listed by Ioannidis (2020a). With a total population of 615,729, this corresponds to a crude frequentist 95% CI for the IFR of [0.44%, 1.49%].

- **$k = 4$ : Split-Dalmatia County, Croatia:** Jerkovic et al. (2020) conducted serological testing for antibodies from April 23rd to April 28th, and obtained a 95% CI for the IR of [0.64%, 2.05%] (from “a representative sample size for the Split-Dalmatia County population, which could reflect a relatively realistic antibody seroprevalence in the county”). This uncertainty interval corresponds to about 12 confirmed cases from 937 tests. The relevant number of deaths is 29 (recorded on May 3rd, 2020), as listed by the Croatian Institute of Public Health ([www.koronavirus.hr](http://www.koronavirus.hr)). With a total population of 447,723, this corresponds to a crude frequentist 95% CI for the IFR of [0.22%, 1.47%].
- **$k = 5$ : Zurich, Switzerland (May):** Emmenegger et al. (2020) estimate a 95% CI for the IR of [0.6%, 1.8%] for “the first half of April 2020” and note that “the prevalence reported here is truly representative of the population under study.” This uncertainty interval corresponds to about 13 confirmed cases from 1,166 tests. The relevant number of deaths is 127 (recorded on May 15th, 2020), as listed by Ioannidis (2020a). With a total population of 1,520,968, this corresponds to a crude frequentist 95% CI for the IFR of [0.39%, 1.66%].